Delft University of Technology

Discrete lattice fracture modelling of hydrated cement paste under uniaxial compression at micro-scale

Jiang, Nengdong; Zhang, Hongzhi; Chang, Ze; Schlangen, Erik; Ge, Zhi; Šavija, Branko

Important note
To cite this publication, please use the final published version (if applicable).
Please check the document version above.

Discrete lattice fracture modelling of hydrated cement paste under uniaxial compression at micro-scale

Nengdong Jiang [a], Hongzhi Zhang [a],*, Ze Chang [b], Erik Schlangen [b], Zhi Ge [a], Branko Šavija [b]

[a] School of Qilu Transportation, Shandong University, Jinan, PR China
[b] Microlab, Faculty of Civil Engineering and Geosciences, Delft University of Technology, Delft, the Netherlands

HIGHLIGHTS

- Compressive failure of hydrated cement paste at the micro-scale was simulated.
- Failure behaviour of various specimens were investigated.
- Boundary restraint effect is more significant for specimens with a low slenderness.
- The boundary condition has negligible effect on the Young's modulus.

ARTICLE INFO

ABSTRACT

A combination of laboratory experiments and numerical simulations at multiple length scales can provide in-depth understanding of fracture behaviour of hydrated cement paste (HCP). To that end, the current work presents a numerical study on compressive failure of hydrated cement paste (HCP) at the micro-scale. Virtual specimens consisting of various phases were obtained using a combination of X-ray computed tomography and image segmentation techniques. The discrete lattice fracture model was used for the deformation and fracture analysis of the specimens subjected to uniaxial compression. The input local mechanical properties of each individual phase were taken from the literature in which a micro-scale compression test was conducted for the calibration of the same type model. The influence of slenderness ratios (1 and 2), water-to-cement ratios (0.3, 0.4 and 0.5 respectively) and lateral confinement of the specimen ends (free and restricted) on the failure behaviour were investigated. It has been shown by the current study that the stress–strain response cannot be completely separated from the used boundary conditions. The proposed model provides an effective tool to understand the compressive fracture behaviour of cement paste at the micro-scale.

© 2020 Elsevier Ltd. All rights reserved.

1. Introduction

Concrete is the most widely used substance on Earth. Cement paste is the basic binding material in concrete that glues aggregates together. Accurate prediction of concrete properties therefore depends, to a large extent, on good understanding of behaviour of hydrated cement paste (HCP). Consequently, simulation and prediction of HCP mechanical properties have generated considerable recent research interest.

HCP is a fairly heterogeneous material ranging from nanometers to millimetres [1]. To have an in-depth understanding of its fracture behaviour, simulations and modelling are required at multiple length scales: namely nano-scale, sub-micro-scale,

micro-scale and *meso*-scale [2]. The nano-scale studies the atomic nature of hydration products, e.g. C-S-H. The sub-nano-scale describes C-S-H gel on the scale ranging from tens to hundreds of nanometers. The micro-scale focuses on the HCP matrix consisting of various constituents, most importantly C-S-H, calcium hydroxide, anhydrous cement particles and capillary pores. In pursuit of fundamental understanding of the link between the microstructure and its macroscopic mechanical performance, mechanical models using microstructural information as input are generally used. Such models are therefore considered as microstructure-informed [3]. At the *meso*-scale, HCP is usually considered as a homogeneous and isotropic continuum. This work focuses on investigation the fracture behaviour of HCP at the micro-scale through the microstructure-informed model.

In general, the microstructure-informed models consist of two steps. The first is related with a detailed 3D microstructure, which

---

can be obtained either by simulations or experiments. In the numerical cement hydration models, cement particles are generally assumed as spherical [4,5]. This influences the hydration process modelling of cement [6] and the elastic stiffness estimation of the HCP at early age [7]. Furthermore, the CemHyd3D model [8] allows a direct representation of multiphase, multi-sized and non-spherical cement particles obtained from SEM images. However, it is pointed by [9] that the microstructure in CemHyd3D are distributed very evenly due to the random based algorithm compared with the results obtained by X-ray computed tomography (XCT). Currently, the XCT is becoming a popular approach for 3D microstructure characterization of cementitious materials [10–13]. On the basis of histogram of greyscale levels, different components, such as capillary pores, anhydrous cement particles, inner and outer hydration products can be segmented through a so-called thresholding approach [14]. Since commonly used microstructural models can only describe the real microstructure in a simplified way, this paper adopts the experimental microstructural data as input.

The second step is the use of model to simulate the fracture process. Numerical approaches like finite-element models [15] site-bond model [16,17], phase field model [13], peridynamic (PD) model [18] and lattice-type model [19–22] have been commonly applied to simulate fracture of hydrated cement paste. Most of the simulations focus on the fracture behaviour in tension. Few of the research investigated the compressive fracture behaviour, which is significantly more complex compared to the tensile failure [23]. As the HCP is usually applied to endure compressive stress, it is of great importance to understand its mechanical performance in compression. To this end, an experimental approach has been proposed by the authors [24], wherein micro-scaled sized specimens were prepared by a combination of thin-sectioning and micro-dicing techniques and compressed by a flat-end tip instrumented by a nanoindenter. On the basis of the experimentally obtained load–displacement curve and fracture pattern, a microstructure-informed model has been developed to simulate the fracture behaviour of a micro-cube (100 µm) under compression. However, the influence of the specimen geometry (shape and size) and boundary conditions (the lateral restraint at the specimen ends) on the compressive fracture behaviour has not been reported. As it is well known from fracture mechanics that these two factors have remarkable effect on the fracture process, the current work therefore aims at bridging the aforementioned gap at the micro-scale.

In this research, experimentally obtained microstructures were directly used as input for a lattice-type model for the simulating fracture process of cement pastes. Influence of slenderness ratios (1 and 2), initial water-to-cement ratios (0.3, 0.4 and 0.5 respectively) and lateral confinement of the specimen ends (free and restricted) on the failure behaviour were investigated. It has been shown by the current study that the stress–strain response cannot be completely separated from the used boundary conditions. It is expected that the proposed model would provide an effective tool for understanding the compressive fracture behaviour of cement paste at the micro-scale.

2. Digital specimens

Digital specimens obtained from the authors' previous work [14] were used. Herein, a brief introduction about the process is given. The first step is to obtain grey-scale level based microstructure. This was achieved by scanning a 28 days cured HCP prism with a square cross-section of 400 µm using a Micro X-ray Computed Tomography (XCT) Scanner (Phoenix Nanotom, Boston, MA, USA). The HCP prism was clipped with an in-house device dur-

ing the scanning. The resulting grey-scale level based microstructure has a voxel resolution of 2 µm. Although this resolution is not as high as others reported [13,17], it is sufficient to model the fracture behaviour of hardened cement paste at micro-scale and consider its heterogeneity [25]. The second step entails segmenting individual phases from the grey-scale level based microstructure through a thresholding process. Four phases can be segmented. They are capillary pore (CP), inner hydration product (IHP), outer hydration product (OHP) and anhydrous cement particle (ACP) In order to study the influence of the water-to-cement (w/c) ratio on the compressive fracture behaviour, HCP prisms prepared with w/c ratios of 0.3, 0.4 and 0.5 were scanned. Detailed information of segmented microstructure for each w/c ratio is presented in Table 1. Two sizes of digital specimens were created with respect to each w/c ratio. The first has a cubic shape with size of 100 µm. It was extracted from the segmented microstructure (Fig. 1). The second was a prism with height of 200 µm and a square cross-section of 100 µm, see Fig. 2. This was achieved by creating a mirrored specimen and connecting it with the original specimen at the mirror surface. In this way, the prism has the same amount of each phase as its corresponding cube as shown in Fig. 1. Therefore, the influence of the slenderness can be investigated by the fracture modelling.

3. Model description

Discrete lattice fracture model has been applied to model the fracture behaviour of quasi-brittle materials, such as cementitious materials [26–28] and nuclear graphite [29,30]. In the lattice model, the continuum is discretized as a network of small beam elements. Considering the low ratio of length and height of the small beam elements, a Timoshenko beam element is used to take shear deformation into account [31]. Material heterogeneity can be considered by utilizing an overlay procedure using the digital specimens generated in Section 2. Details on the network generation and overlay procedure is as follows:

Firstly, a sub-cell was defined in the centre of each voxel of the digital specimen. A node was then randomly positioned within each sub-cell. Afterwards, Voronoi tessellation of the domain, as described by [32], was performed to the defined nodes. In this process, nodes in adjacent Voronoi cells were connected with beam elements, see Fig. 3a. Note that the ratio between the sub-cell and the voxel determines the degree of randomness of the lattice system [33]. To consistent with the author' previous work, 0.5 was adopted herein. Furthermore, the mesh configuration that is chosen results in a Poisson's ratio of about 0.18 for the global performance, which is realistic for cementitious materials [34].

The overlay procedure was conducted to assign beam element type according to the position of its end nodes, see Fig. 3b. The resulting element type spatial distribution for cubic specimen with w/c ratio of 0.3 is shown in Fig. 4 as an example. This was further used to define mechanical properties of each lattice element. This way different mechanical properties can be assigned to their corresponding phases. A Reuss model was then used to determine the elastic modulus of element i-j following:

$$\frac{2}{E_{i\text{-}j}} = \frac{1}{E_i} + \frac{1}{E_j}, \tag{1}$$

Table 1
Details of segmented microstructures of HCP cured for 28 days, after [25].

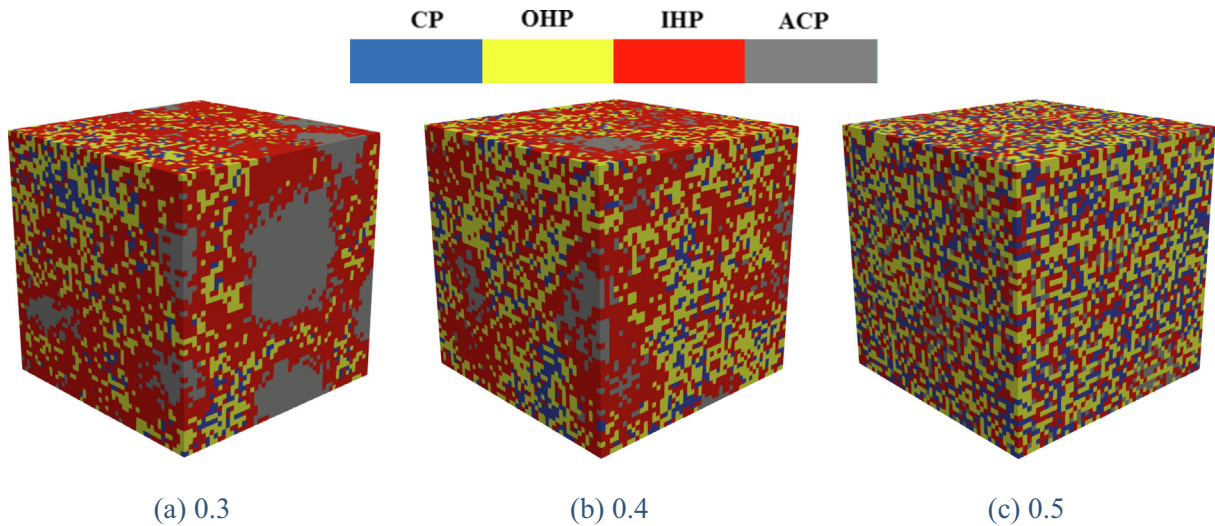| W/c	CP (%)	ACP (%)	Hydration degree (%)
0.3	8.44	15.30	69.65
0.4	11.84	10.64	74.99
0.5	17.50	8.02	80.85

Fig. 1. HCP cubic specimens (100 μm) with various w/c ratio (CP: capillary pore; IHP: inner hydration product; OHP: outer hydration product; ACP: anhydrous cement particle).
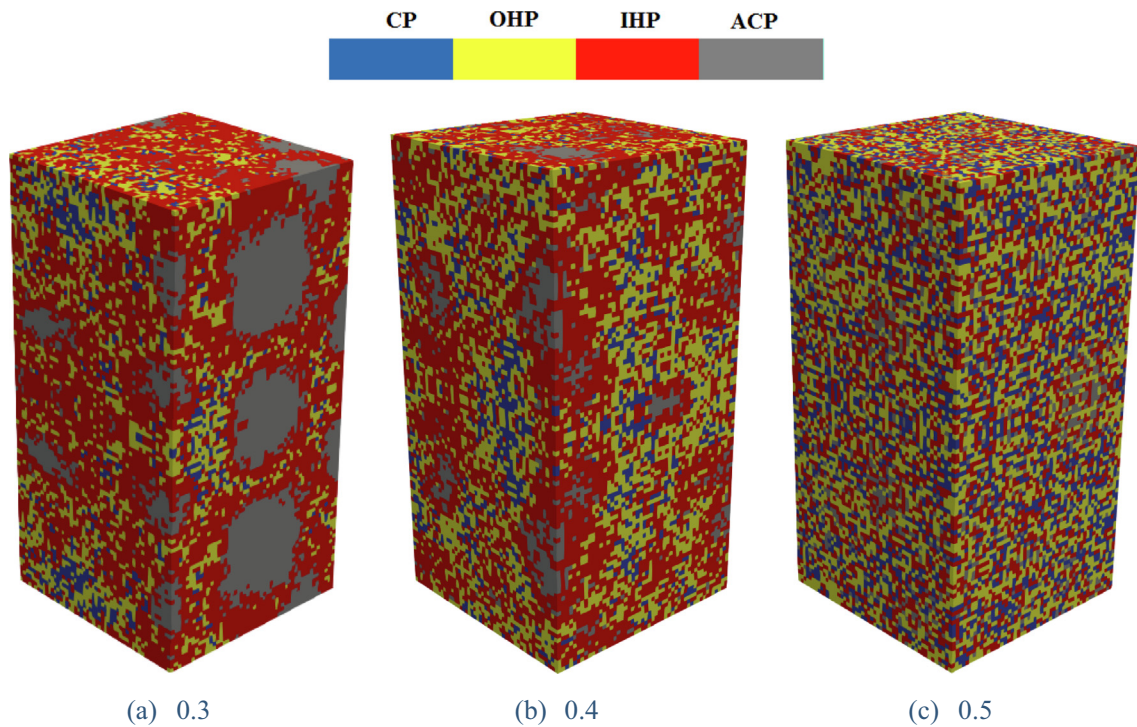

Fig. 2. HCP prismatic specimen (100 μm × 100 μm × 200 μm) with different w/c ratios (CP: capillary pore; IHP: inner hydration product; OHP: outer hydration product; ACP: anhydrous cement particle).

where E_i and E_j are respectively elastic moduli of phases i and j. No element is created in the mesh when either voxel i or voxel j is a pore voxel. The strength of element i-j is adopted as the smaller value in between phases i and j, for both compressive and tensile. The assigned mechanical properties of each phase are shown in Table 2. Elastic modulus of each phase was derived from nanoindentation experiments [35]. Tensile and compressive strengths were taken from the authors previous works [14,24], wherein micro-scale experiments were developed for the purpose of calibration. The same values have been successfully used to simulate the fracture process of the micro-scale sized specimens under different test configurations, such as one-sided splitting test [36], 3-point bending test [37] and uniaxial compression test [24] by the authors.

These parameters were adopted in the current work constantly. It is worth mentioning that the input mechanical properties of different phases are dependent on the resolution of the discrete model: a coarser mesh corresponds to the lower input mechanical properties since larger pores and defects are homogenized in the domain represented by the element or voxel.

The specimen was subjected to a unit displacement on the one end, while it is clamped at the other end to mimic the uniaxial compression loading. As it is well-known that, for cementitious materials under uniaxial compression, the test results strongly depend on the frictional restraint between specimen and loading platen. This is induced by the lateral deformation of the specimen ends. In order to study the exact influence of this confinement on
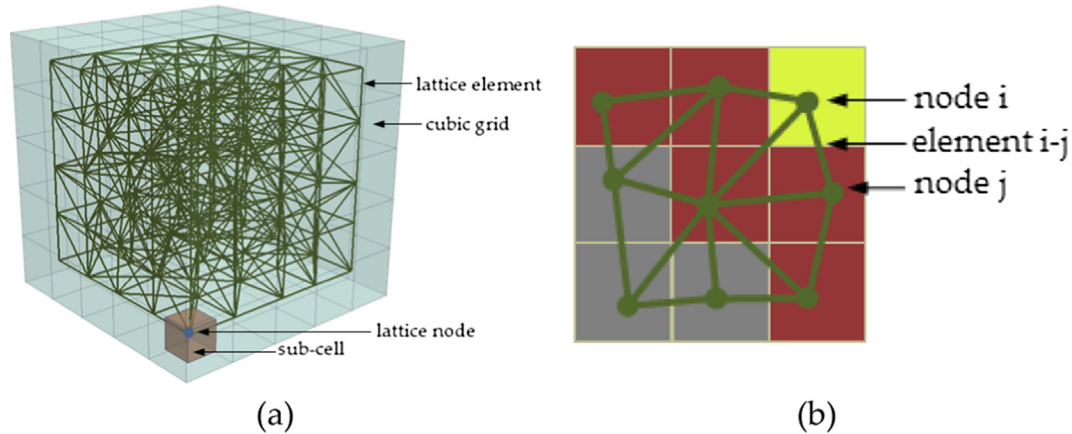
Fig. 3. Schematic view of lattice model generation: (a) Node and network generation procedure (5 × 5 × 5); (b) an example of the overlay procedure for HCP, shown in 2D for simplicity, after [14].
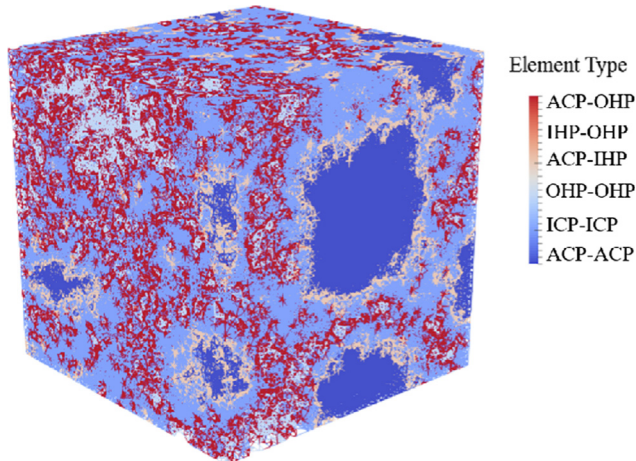

Fig. 4. Element type spatial distribution of cubic specimen with w/c ratio of 0.3.

Table 2
Assigned local mechanical properties of individual phases at micro-scale.

Phase	Young's modulus (GPa) [35]	Tensile strength (MPa) [14]	Compressive strength (MPa) [24]
AHC	99	683	6830
INP	31	92	920
OHP	25	58	580

Table 3
Configurations of the simulated specimens.

Sample name	W/c ratio	Slenderness ratio	Lateral restraint
WC03CR	0.3	1	Restricted
WC03CF	0.3	1	Free
WC03PR	0.3	2	Restricted
WC03PF	0.3	2	Free
WC04CR	0.4	1	Restricted
WC04CF	0.4	1	Free
WC04PR	0.4	2	Restricted
WC04PF	0.4	2	Free
WC05CR	0.5	1	Restricted
WC05CF	0.5	1	Free
WC05PR	0.5	2	Restricted
WC05PF	0.5	2	Free

the fracture behaviour and stress–strain responses, simulations were carried out under both free and confined boundary conditions for each specimen. This results in 12 simulations as listed in Table 3. In case of the free lateral boundary condition, no restriction was applied to the nodes on the two ends, while the degree of freedom of lateral movements and rotations was fixed for the restricted boundary conditions. A set of linear elastic analysis is then performed by calculating the stress within each element following [19]:

$$\sigma = \frac{N}{A} + \alpha_M \frac{\max(M_X, M_Y)}{W}, \qquad (2)$$

where A is cross-sectional area of the element; W is the second moment of cross-sectional area; α_M is the bending influence factor. As shown in the authors' previous work, a small value (i.e. 0.05) is suitable for modelling the fracture behaviour of material in tension [14], while a large α_M (i.e. 0.5) is recommended for the element in compression to depict the failure caused by bending [38]. Therefore, in the current study the α_M was adopted as 0.05 when the beam is under tension, while 0.5 was used for a beam under compression. Loading is increased until exactly one element in the mesh has a stress/strength ratio equal to one. This is achieved through a so-called using a sequentially-linear solution procedure [19,39]. A method consisting in removing the element stiffness stepwise was adopted as described previously in the authors previous work [24]. First the bending and shear stiffness would be removed and only if that same element fails again, the remaining axial stiffness would be removed, see Fig. 5. In order to avoid the overlapping of the adjacent nodes and to account for the sliding that happened in between the two surfaces of a crack, the truss element was allowed to fail only in tension. The network is then updated and updated and relaxed. The calculation procedure is repeated until a predefined displacement (0.02 strain in the current study) is met. Consequently, the fracture pattern and load–displacement response can be obtained.

4. Results and discussions

4.1. Stress–strain responses

The simulated stress–strain response of all the specimens are shown in Fig. 6, based on which the Young's modulus and compressive strength can be computed. The calculated mechanical properties are listed in Table 4. Clearly, the w/c ratio plays a dominating role on the mechanical properties of HCP. With the w/c ratio increasing, both the compressive strength and Young's mod-
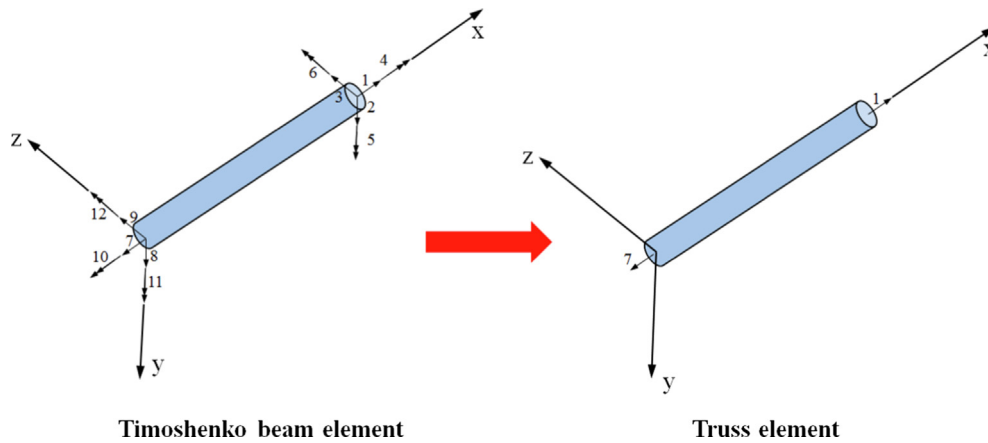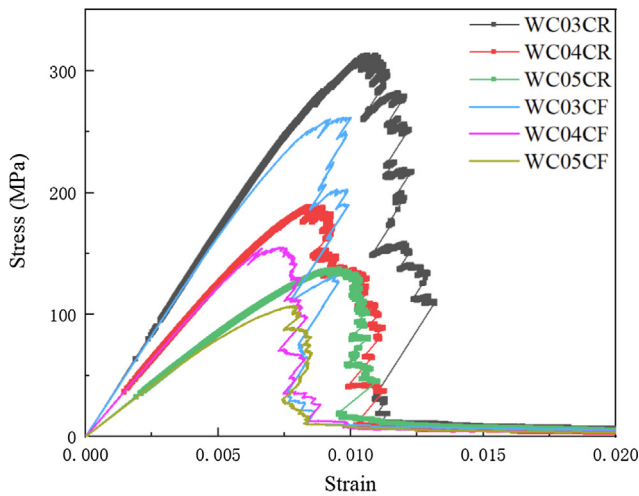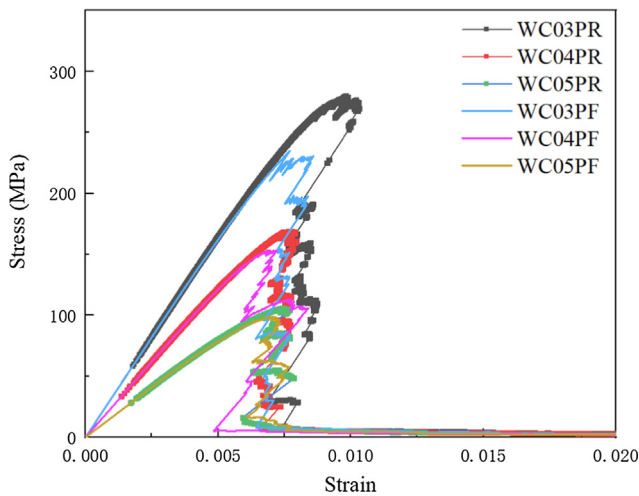
Timoshenko beam element   **Truss element**

Fig. 5. Schematic view of the element degradation at first step [24].

(a) cubic specimens

(b) prismatic specimens.

Fig. 6. Simulated stress–strain response of all the specimens.

Table 4
Summary of the simulated Young's moduli and compressive strengths.

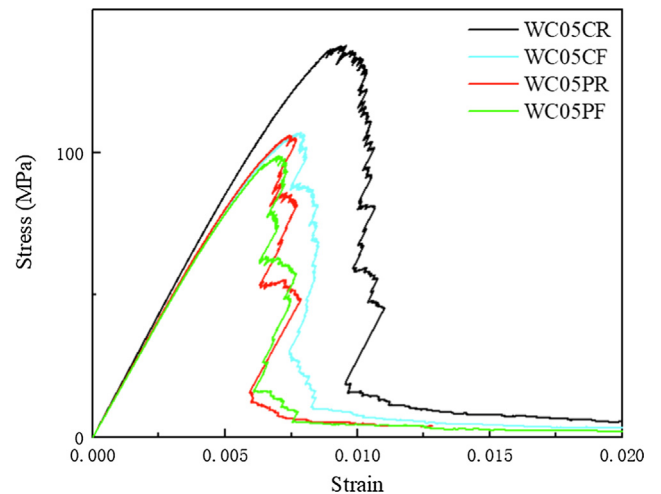| Sample	Young's modulus (GPa)	Compressive strength (MPa)
WC03CR	34.20	313.06
WC03CF	33.27	261.78
WC03PR	33.27	280.06
WC03PF	32.84	234.96
WC04CR	25.73	189.66
WC04CF	25.16	154.98
WC04PR	25.05	169.04
WC04PF	24.82	153.27
WC05CR	17.39	137.89
WC05CF	16.69	107.05
WC05PR	16.66	106.05
WC05PF	16.40	98.75

Fig. 7. Comparison of stress–strain response of specimens with w/c ratio of 0.5.

In general, the simulated compressive strength of HCP seems to be very high compared to the macroscopic values of such material or normal concrete, which are measured at the millimetre level [40]. Even for the HCP with w/c ratio of 0.5, the compressive strength can be as high as 98.75 MPa. the compressive strength of the 100 μm HCP cube specimens have recently been measured experimentally and compressive strengths are 159. 52 ± 31.90 MP a, 124.97 ± 24.99 MPa and 110.24 ± 40.788 MPa for w/c ratio of 0.3, 0.4 and 0.5 respectively [24], which are in the same order with the
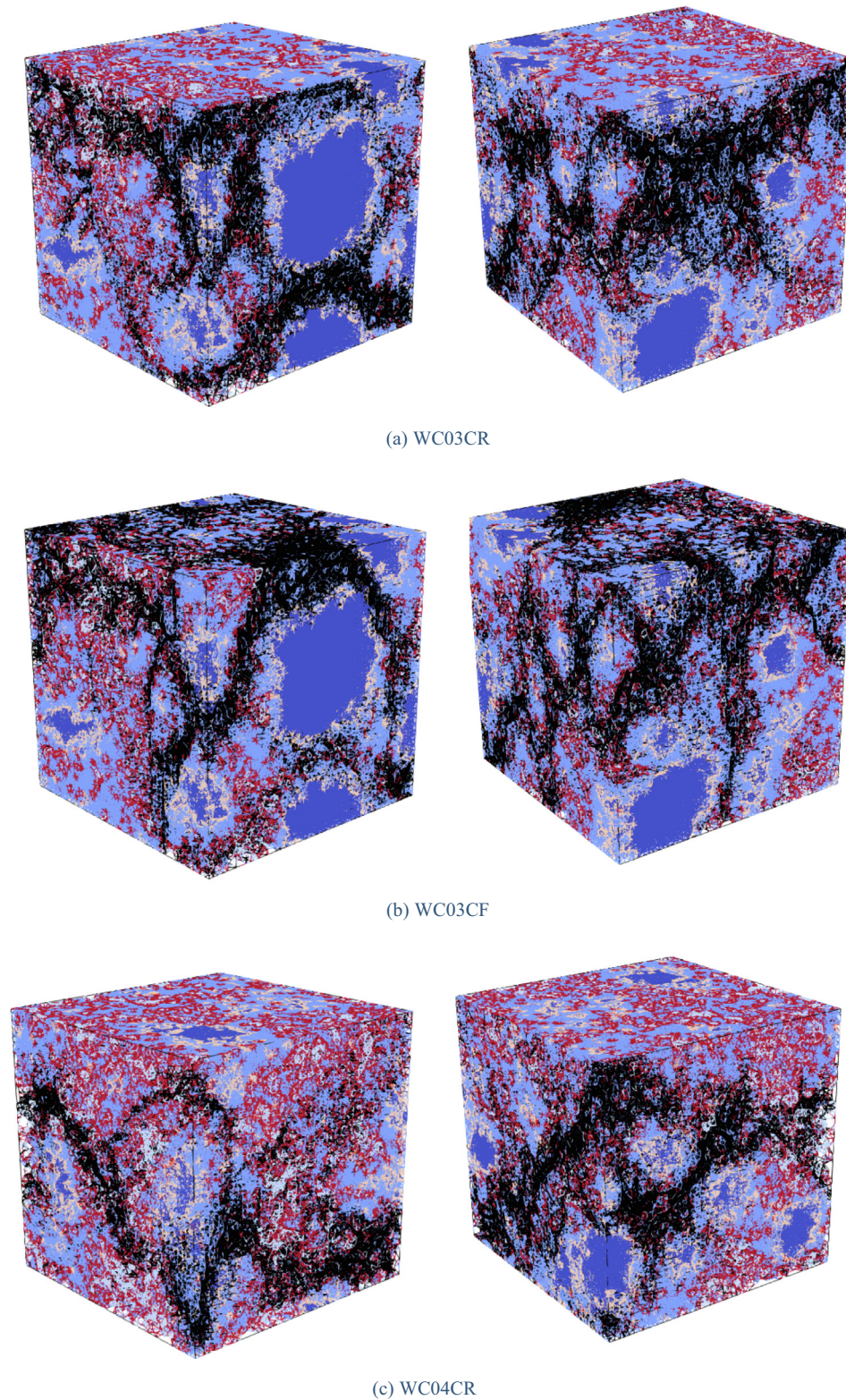
ulus decrease, as the HCP prepared with lower w/c ratio has less porosity and higher amount of ACP, which acts as stiff inclusions in the matrix.

(a) WC03CR

(b) WC03CF

(c) WC04CR

Fig. 8. Simulated crack pattern of cubic specimens at the failure stage (black-crack).

simulated results. In terms of the w/c ratio of 0.3 and 0.4, the simulated strengths are much higher than the experimentally measured mean value. However, some of the specimens that have been measured in [40] have the similar strength. This can be attributed to the deviation of the statistics as the number of the investigated digital specimens might not be large enough to represent the stochastic nature of cement paste at this scale. Compared with the

measured compressive strength of C-S-H pillar having a diameter of a few micrometres (838 ± 244 MPa for 0.5 μm and 465 ± 147. 6 MPa for 2.5 μm), the simulated values of the micro-scale sized specimens are much lower [41]. This is consistent with the so-called size effect [42,43]. Likewise, the splitting strength follows the same trend [44]. This is mainly because that the small sized samples have no defects greater than the sample size introducing
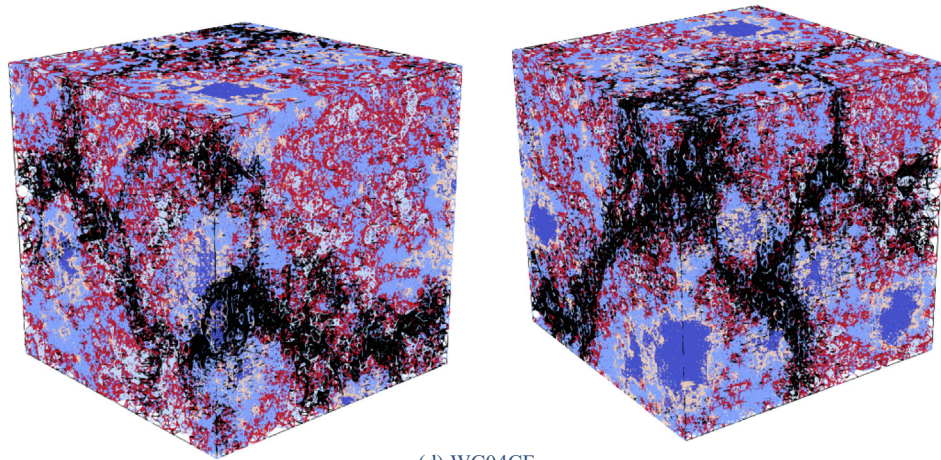
(d) WC04CF
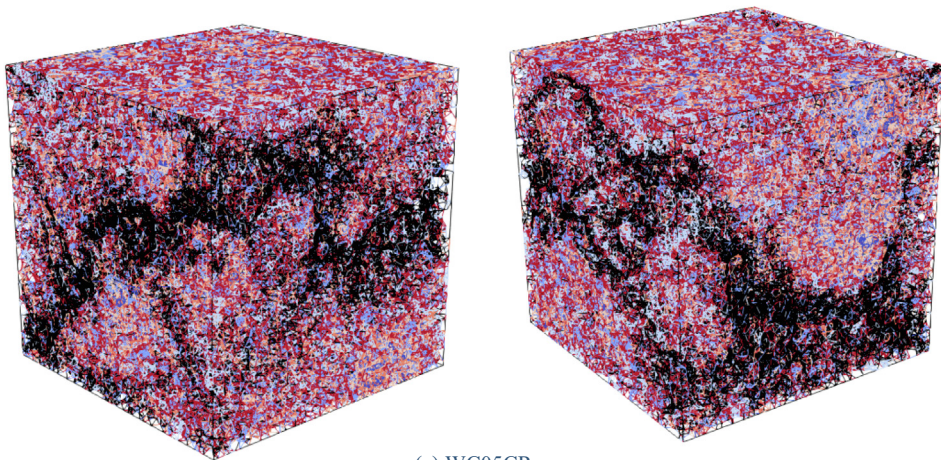
(e) WC05CR
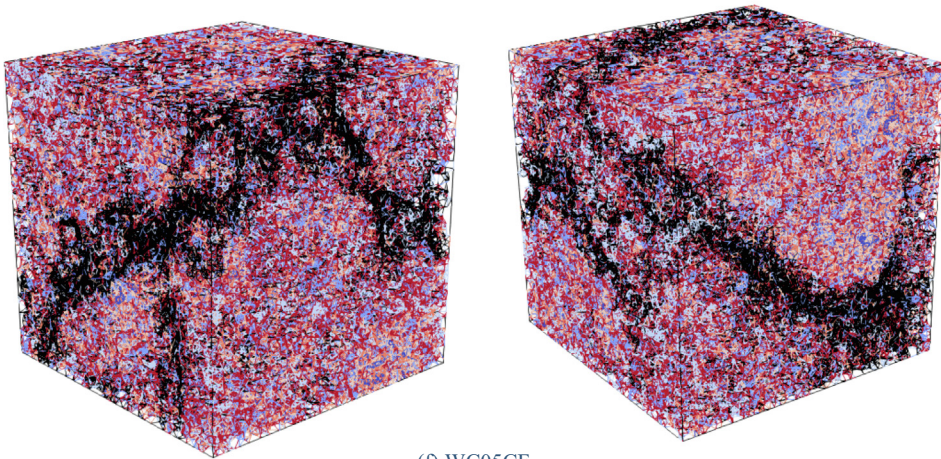
(f) WC05CF

Fig. 8 (continued)

stress concentration and reducing material strength [44–46]. The compressive strength derived from the cubic specimen under restricted boundary are compared with the tensile strength derive from exactly same virtual specimens [14]. It is found that the ratio of compressive/tensile strength ranging from 7.91 to 9.66 is in accordance with concrete [40].

Regardless of the w/c ratio, both the specimen geometry and the horizontal confinement of the specimen ends have influence on the load–displacement responses of the material. Under the same loading configuration, the specimens with higher slenderness ratio (prismatic specimen) have lower compressive strength and more brittle softening behaviour. Furthermore, the influence of the boundary restraint is more significant for specimens with a low slenderness. In terms of w/c ratio of 0.5, the WC05CR has higher strength and ductility while the others have a similar stress–strain response, see Fig. 7. This indicates two things: for a prism there is no influence of the boundary conditions (fixed or free) on the strength and the strength is similar for a prism and
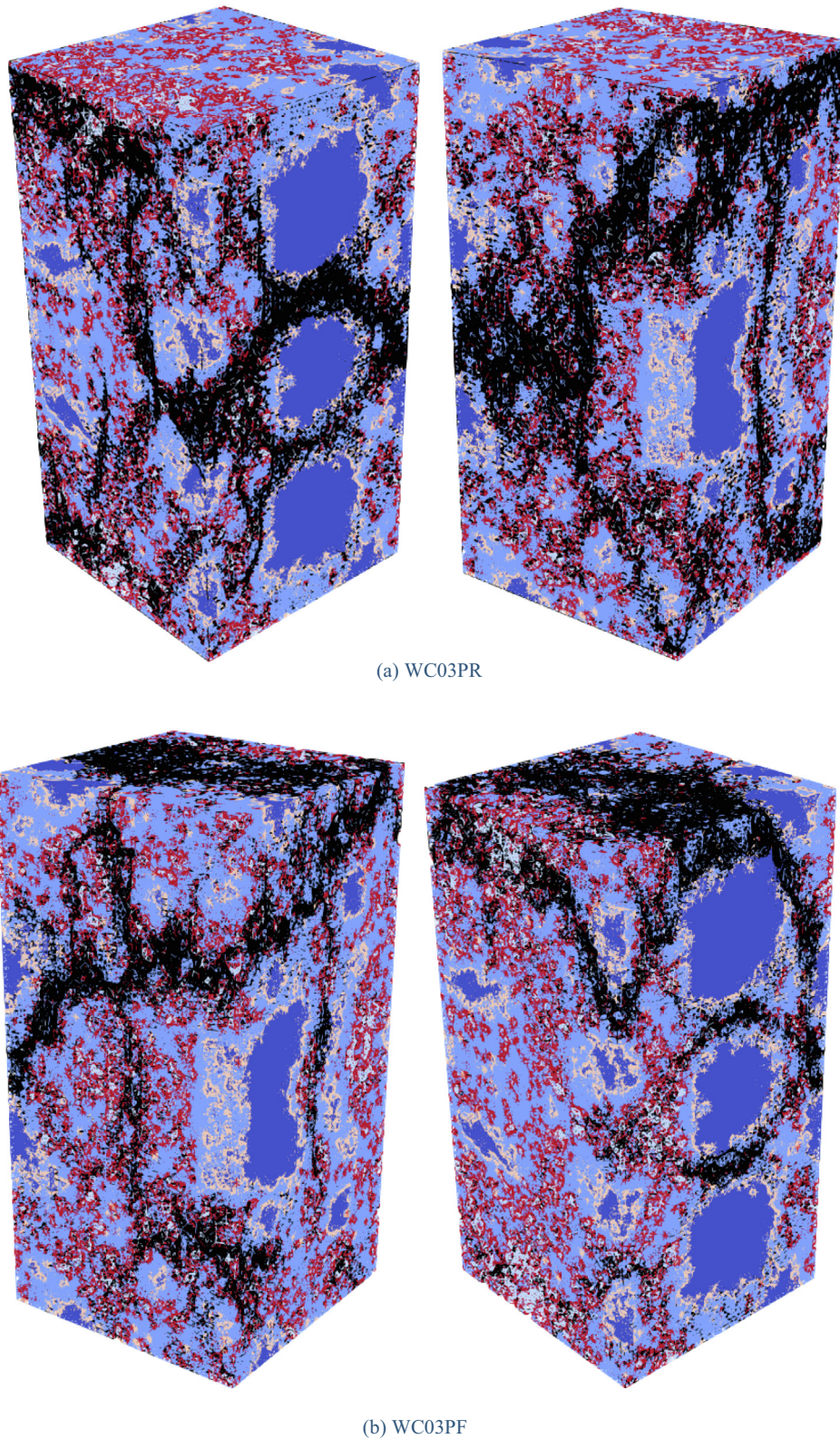
(a) WC03PR

(b) WC03PF

Fig. 9. Simulated crack pattern of prismatic specimens at the failure stage (black-crack).

cube with free boundaries. This trend has also been observed in the concrete level [38]. However, this is not so pronounced for specimens with w/c ratio of 0.4 and 0.3 due the material heterogeneity. For example, the shape of the pore and anhydrous cement particle at the mirror surface of the cube would change in the correspond-

ing prism although the proportions remain the same. Furthermore, it should be mentioned that the specimen geometry and the boundary restraint have limited influence on the simulated Young's modulus which is influenced by the properties of material components and their relative amounts.
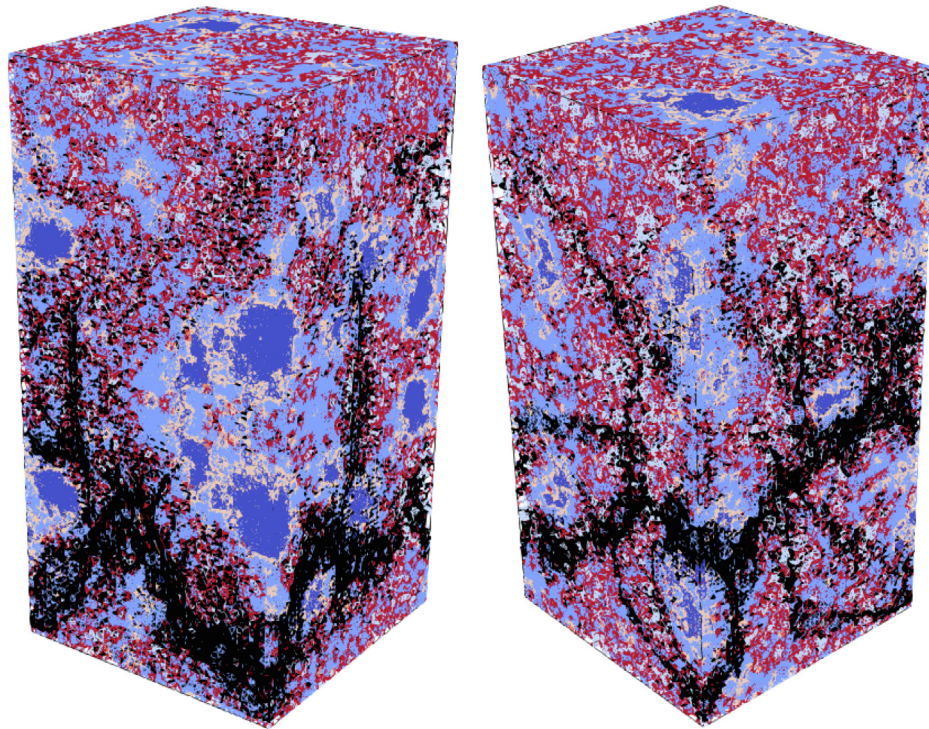
(c) WC04PR
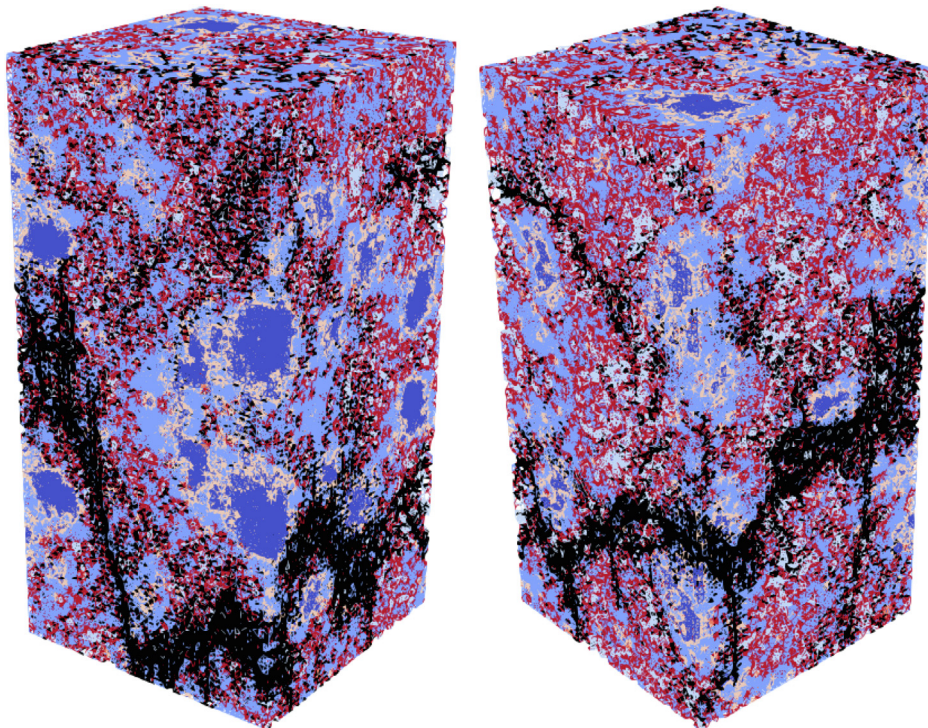
(d) WC04PF

Fig. 9 (*continued*)

4.2. Crack pattern

The simulated crack patterns of the specimens at the failure state are shown in Figs. 8 and 9. Due to the confinement near the boundaries, no crack is observed on the restricted surfaces. As explained in the literature [38,47–49], due to confinement at the two ends of the specimen, an area under triaxial compression

occurs, see Fig. 10 and HCP has much higher resistance to compression than tension. Thus, the cracks occur mainly in the area outside the cone shaped area. Furthermore, a larger relative restrained area occurs in the specimen with small slenderness. This results in a higher strength obtained for the cubic specimens.

Furthermore, the inclined major cracks on the specimen's outer layers follow a tortuous path and seem to be deflected by the ACP.
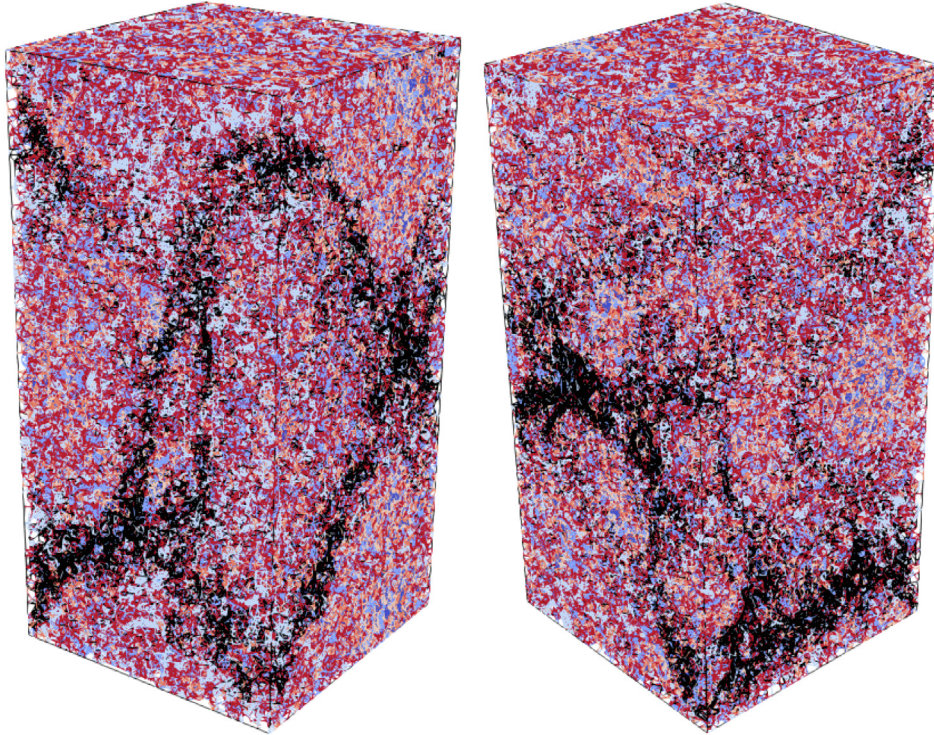
(e) WC05PR
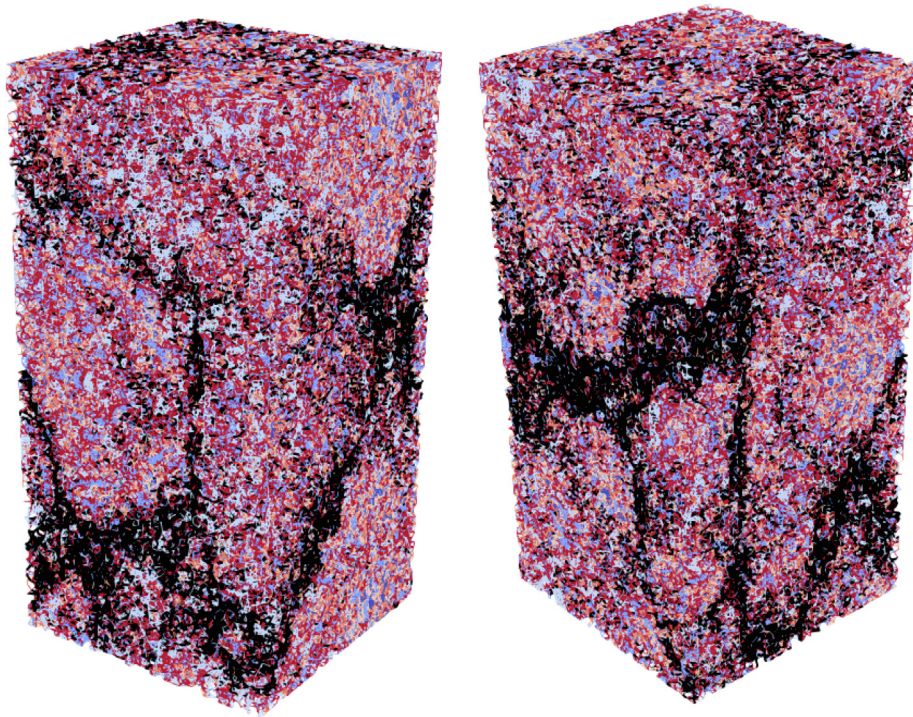
(f) WC05PF

Fig. 9 (*continued*)

This is because that ACP has the highest stiffness and strength, behaving as a stiff inclusion in the matrix. Consequently, the crack propagates bypass the ACP. As HCP with higher w/c ratio has less amount and smaller sized ACP, the cracks can easily localize and coalesce. This leads to a lower strength and more brittle softening behaviour.

Another observation is that the major cracks in the prismatic specimens with no lateral confinement tend to be more vertical
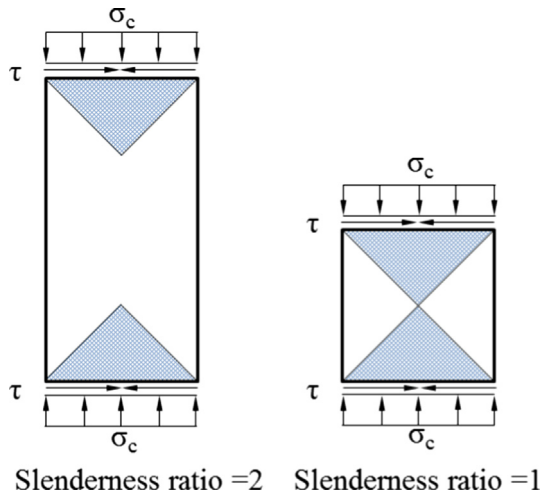
Fig. 10. Confined zones caused by frictional confinement [24].

than the others. Similar observation has also been found for concrete at the *meso*-scale [38], see Fig. 11. Furthermore, when frictional restraint between specimen and loading platen is effectively reduced, a axial splitting failure mode is observed for a centimetre sized HCP specimen [50]. However, this can hardly be achieved at the micro-scale, as the heterogeneity of the material causes significant stress concentration and deflects the crack propagation.

4.3. General discussion

Under the hierarchical modelling scheme [3,15], a so-called uncoupled volume averaging upscaling method [37,44,51] can be applied to bridge the micro and meso scales. In this upscaling method, the simulated global mechanical performance of composites at lower scale are directly assigned as the local mechanical properties of the matrix in the upper scale models. However, as it has been demonstrated in the current study that the stress–strain response of the material cannot be separated from the boundary conditions as well as the specimen size, attention has to be paid when this uncoupled volume averaging upscaling
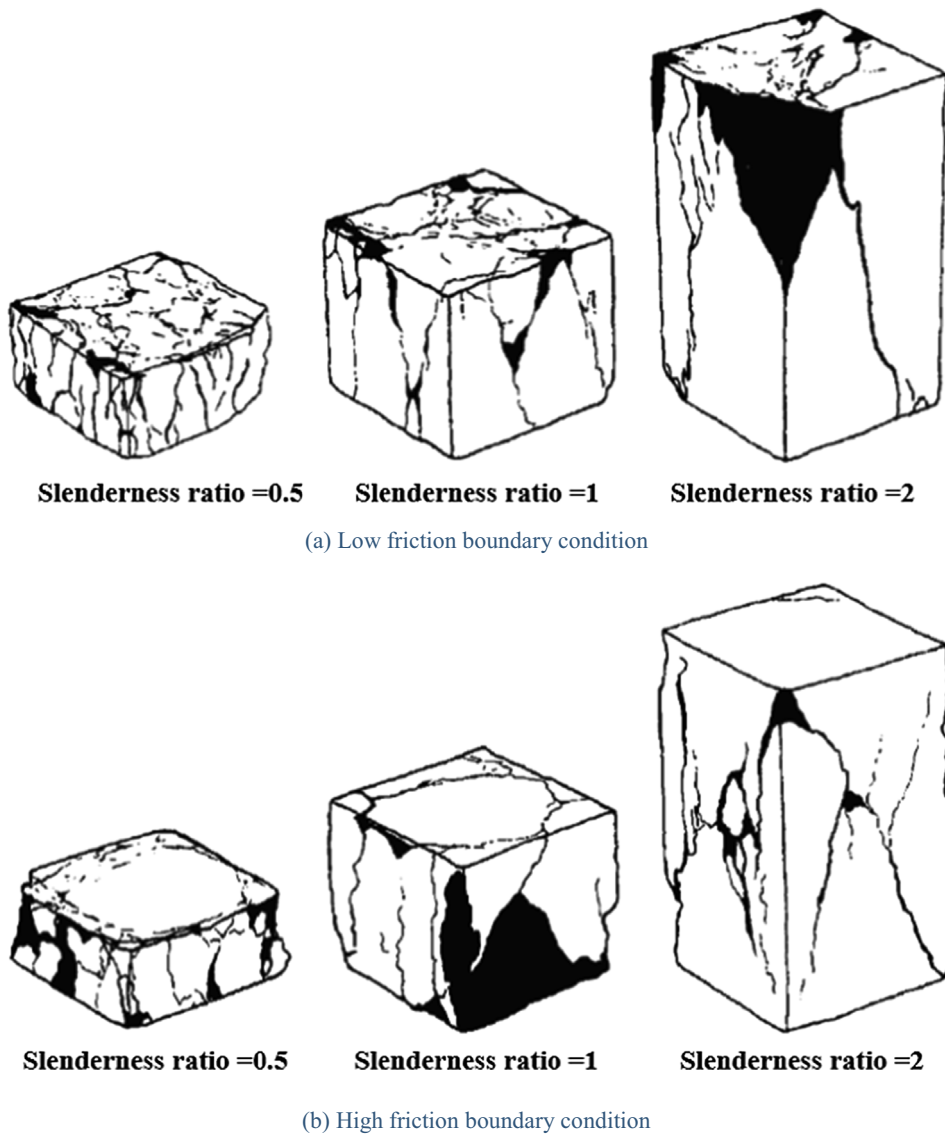

(a) Low friction boundary condition

(b) High friction boundary condition

Fig. 11. Crack pattern of concrete specimens at the failure stage under compression [38].

method is used. One of the most concerned issue is that the volume size of material structure at small scale has to match the smallest feature of the larger scale observation. The others are the boundary conditions that used to obtain the constitutive relation of the material at the smaller scale. As it is more plausible to use the "realistic" value as input in a model, free confinement at the ends is suggested in both uniaxial tension and compression simulations. Furthermore, with recent advances in the nano-scale and sub-nano-scale modelling, the results from atomistic simulations [52–57], can be utilized as input for the current micro-scale model. Likewise, the material volume of different phases should match the resolution of the micro-scale model. This enables that the model has fully predictive capabilities at the *meso*-scale and offers the opportunity of investigating in more detail the influence of the microstructure on the material response and engineering properties.

For each type of mixture, only one digital specimen was used for the study. This can also be a source leading to the dispersion of the reported micromechanical properties of HCP in the literature [24,58,59]. Considering the heterogeneous nature of HCP at the micro-scale, stochastic-based approach is required for an in-depth understanding. This can be achieved by randomly extracting digital specimens from the segmented microstructure at different positions and performing the computational compression tests on them, similar like the references [25,30]. However, in comparison to tensile failure, compressive fracture is at least one step up in the degree of complexity [23] and more (micro) cracks form before the specimen fails. Consequently, the modelling of compressive failure requires significantly more computational time. More power computational facilities and efficient numerical algorithm are therefore expected in the future to overcome the aforementioned limitations.

5. Conclusions

The current work presents a numerical study on the compressive failure of HCP at the micro-scale. The microstructure informed discrete lattice fracture model was used for the deformation and fracture analysis of the specimens in compression. Influence of slenderness ratios, initial water to cement ratios and lateral confinement of the specimen ends on the failure behaviour were investigated. The following conclusions can be drawn:

- With the decrease of w/c ratio, the compressive strength and Young's modulus increase and the softening regime become more ductile.
- The simulated compressive strength of HCP at the micro-scale is found to be lower than the measured strength of C-S-H, but higher than the compressive strength of HCP at the *meso*-scale. This is in accordance with the size effect for quasi-brittle materials.
- For specimens with restrained boundaries, higher slenderness results in lower compressive strength and more brittle softening behaviour. The influence of the boundary restraint is more significant for specimens with a low slenderness. For higher slenderness the influence of boundary restraint seems to disappear. The specimen geometry and the boundary restraint have limited influence on the simulated Young's modulus. These findings are in accordance with the findings in concrete.
- Inclined major cracks on the specimen's surface that follow a tortuous path and are deflected by the ACP are observed at the failure stage. Similar to the observation at the *meso*-scale, the major cracks in the prismatic specimens with no lateral confinement at the boundaries tend to be more vertical than the for cubic specimens.

CRediT authorship contribution statement

Nengdong Jiang: Investigation, Writing - original draft. **Hongzhi Zhang:** Funding acquisition, Methodology, Supervision, Writing - review & editing. **Ze Chang:** Investigation, Writing - original draft. **Erik Schlangen:** Methodology, Writing - review & editing. **Zhi Ge:** Funding acquisition, Writing - review & editing. **Branko Šavija:** Methodology, Writing - review & editing.

Declaration of Competing Interest

The authors declare that they have no known competing financial interests or personal relationships that could have appeared to influence the work reported in this paper.

References

[1] J.G. Van Mier, Concrete fracture: a multiscale approach, CRC press2012.
[2] J.S. Dolado, K. Van Breugel, Recent advances in modeling for cementitious materials, Cem. Concr. Res. 41 (7) (2011) 711–726.
[3] H. Zhang, Y. Xu, Y. Gan, Z. Chang, E. Schlangen, B. Šavija, Microstructure informed micromechanical modelling of hydrated cement paste: Techniques and challenges, Constr. Build. Mater. 251 (2020).
[4] S. Bishnoi, K.L.J.C. Scrivener, c. research, μic: A new platform for modelling the hydration of cements, 39(4) (2009) 266-274.
[5] K. Van Breugel, Numerical simulation of hydration and microstructural development in hardening cement-based materials:(II) applications, Cem. Concr. Res. 25 (3) (1995) 522–530.
[6] J.W. Bullard, E.J. Garboczi, A model investigation of the influence of particle shape on portland cement hydration, Cem. Concr. Res. 36 (6) (2006) 1007–1015.
[7] B. Pichler, C. Hellmich, J. Eberhardsteiner, Spherical and acicular representation of hydrates in a micromechanical model for cement paste: prediction of early-age elasticity and strength, AcMec 203 (3) (2009) 137–162.
[8] D.P. Bentz, CEMHYD3D: A three-dimensional cement hydration and microstructure development modelling package. Version 2.0, US Department of Commerce, National Institute of Standards and Technology2000.
[9] M. Hain, P. Wriggers, Numerical homogenization of hardened cement paste, CompM 42 (2) (2008) 197–212.
[10] T. Chotard, M. Boncoeur-Martel, A. Smith, J. Dupuy, C. Gault, Application of X-ray computed tomography to characterise the early hydration of calcium aluminate cement, Cem. Concr. Compos. 25 (1) (2003) 145–152.
[11] M.A.B. Promentilla, T. Sugiyama, T. Hitomi, N. Takeda, Quantification of tortuosity in hardened cement pastes using synchrotron-based X-ray computed microtomography, Cem. Concr. Res. 39 (6) (2009) 548–557.
[12] M. Zhang, Y. He, G. Ye, D.A. Lange, K. van Breugel, Computational investigation on mass diffusivity in Portland cement paste based on X-ray computed microtomography (μCT) image, Constr. Build. Mater. 27 (1) (2012) 472–481.
[13] T.-S. Han, X. Zhang, J.-S. Kim, S.-Y. Chung, J.-H. Lim, C. Linder, Area of lineal-path function for describing the pore microstructures of cement paste and their relations to the mechanical properties simulated from μ-CT microstructures, Cem. Concr. Compos. 89 (2018) 1–17.
[14] H. Zhang, B. Šavija, S. Chaves Figueiredo, M. Lukovic, E. Schlangen, Microscale testing and modelling of cement paste as basis for multi-scale modelling, Materials 9 (11) (2016) 907.
[15] F. Bernard, S. Kamali-Bernard, W. Prince, 3D multi-scale modelling of mechanical behaviour of sound and leached mortar, Cem. Concr. Res. 38 (4) (2008) 449–458.
[16] M. Zhang, A.P. Jivkov, Microstructure-informed modelling of damage evolution in cement paste, Constr. Build. Mater. 66 (2014) 731–742.
[17] M. Zhang, A.P. Jivkov, Micromechanical modelling of deformation and fracture of hydrating cement paste using X-ray computed tomography characterisation, Compos. Part B Eng. 88 (2016) 64–72.
[18] D. Hou, W. Zhang, P. Wang, H. Ma, Microscale peridynamic simulation of damage process of hydrated cement paste subjected to tension, Constr. Build. Mater. 228 (2019) 117053.
[19] Z. Qian, Multiscale modeling of fracture processes in cementitious materials, Delft University of Technology, Delft, The Netherlands, 2012.

[20] M. Luković, E. Schlangen, G. Ye, Combined experimental and numerical study of fracture behaviour of cement paste at the microlevel, Cem. Concr. Res. 73 (2015) 123–135.

[21] B. Šavija, H. Zhang, E. Schlangen, Micromechanical testing and modelling of blast furnace slag cement pastes, Constr. Build. Mater. 239 (2020) 117841.

[22] H. Zhang, B. Šavija, M. Luković, E. Schlangen, Experimentally informed micromechanical modelling of cement paste: an approach coupling X-ray computed tomography and statistical nanoindentation, Compos. Part B Eng. 157 (2019) 109–122.

[23] J.G. Van Mier, Fracture processes of concrete, CRC press 2017.

[24] H. Zhang, Y. Xu, Y. Gan, Z. Chang, E. Schlangen, B. Šavija, Combined experimental and numerical study of uniaxial compression failure of hardened cement paste at micrometre length scale, Cem. Concr. Res. 126 (2019) 105925.

[25] H. Zhang, B. Šavija, E. Schlangen, Towards understanding stochastic fracture performance of cement paste at micro length scale based on numerical simulation, Constr. Build. Mater. 183 (2018) 189–201.

[26] L.-Y. Lv, H. Zhang, E. Schlangen, Z. Yang, F. Xing, Experimental and numerical study of crack behaviour for capsule-based self-healing cementitious materials, Constr. Build. Mater. 156 (2017) 219–229.

[27] E. Schlangen, E. Garboczi, Fracture simulations of concrete using lattice models: computational aspects, Eng. Fract. Mech. 57 (2) (1997) 319–332.

[28] G. Lilliu, J.G. van Mier, 3D lattice type fracture model for concrete, Eng. Fract. Mech. 70 (7–8) (2003) 927–941.

[29] B. Šavija, G.E. Smith, P.J. Heard, E. Sarakinou, J.E. Darnbrough, K.R. Hallam, E. Schlangen, P.E. Flewitt, Modelling deformation and fracture of Gilsocarbon graphite subject to service environments, JNuM (2017).

[30] B. Šavija, D. Liu, G. Smith, K.R. Hallam, E. Schlangen, P.E. Flewitt, Experimentally informed multi-scale modelling of mechanical properties of quasi-brittle nuclear graphite, Eng. Fract. Mech. 153 (2016) 360–377.

[31] E. Schlangen, Z. Qian, 3D modeling of fracture in cement-based materials, J. Multiscale Modell. 1 (02) (2009) 245–261.

[32] M. Yip, J. Mohle, J. Bolander, Automated modeling of three-dimensional structural components using irregular lattices, Comput. Aided Civil Infrastruct. Eng. 20 (6) (2005) 393–407.

[33] E. Schlangen, J.G.M. van Mier, Experimental and numerical analysis of micromechanisms of fracture of cement-based composites, Cem. Concr. Compos. 14 (2) (1992) 105–118.

[34] P.K. Mehta, P.J. Monteiro, Microstructure and properties of hardened concrete, Concr. Microstruct. Propert. Mater. (2006) 41–80.

[35] C. Hu, Z. Li, Micromechanical investigation of Portland cement paste, Constr. Build. Mater. 71 (2014) 44–52.

[36] H. Zhang, B. Šavija, E. Schlangen, Combined experimental and numerical study on micro-cube indentation splitting test of cement paste, Eng. Fract. Mech. 199 (2018) 773–786.

[37] H. Zhang, B. Šavija, S.C. Figueiredo, E. Schlangen, Experimentally validated multi-scale modelling scheme of deformation and fracture of cement paste, Cem. Concr. Res. 102 (2017) 175–186.

[38] M.A. van Vliet, J.M. van Mier, Experimental investigation of concrete fracture under uniaxial compression, mechanics of cohesive-frictional materials: an international journal on experiments, Modell. Comput. Mater. Struct. 1 (1) (1996) 115–127.

[39] E. Schlangen, Experimental and Numerical Analysis of Fracture Processes in Concrete, Delft University of Technology, 1993.

[40] A.M. Neville, Properties of concrete, Pearson Education India1963.

[41] R. Shahrin, C.P. Bobko, Micropillar compression investigation of size effect on microscale strength and failure mechanism of Calcium-Silicate-Hydrates (C-S-H) in cement paste, Cem. Concr. Res. 125 (2019) 105863.

[42] Z.P. Bažant, Size effect in blunt fracture: concrete, rock, metal, J. Eng. Mech. 110 (4) (1984) 518–535.

[43] A. Carpinteri, B. Chiaia, G. Ferro, Size effects on nominal tensile strength of concrete structures: multifractality of material ligaments and dimensional transition from order to disorder, Mater. Struct. 28 (6) (1995) 311.

[44] H. Zhang, B. Šavija, Y. Xu, E. Schlangen, Size effect on splitting strength of hardened cement paste: experimental and numerical study, Cem. Concr. Compos. 94 (2018) 264–276.

[45] D. Liu, B. Šavija, G.E. Smith, P.E. Flewitt, T. Lowe, E. Schlangen, Towards understanding the influence of porosity on mechanical and fracture behaviour of quasi-brittle materials: experiments and modelling, Int. J. Fract. (2017) 1–16.

[46] D. Liu, K. Mingard, O.T. Lord, P. Flewitt, On the damage and fracture of nuclear graphite at multiple length-scales, JNuM 493 (2017) 246–254.

[47] K.H. Gerstle, D.L. Linse, P. Bertacchi, Strength of concrete under multiaxial stress states, Spec. Publ. 55 (1978) 103–132.

[48] M. Kotsovos, Effect of testing techniques on the post-ultimate behaviour of concrete in compression, Mater. Constr. 16 (1) (1983) 3–12.

[49] J.G.M. Van Mier, Strain-softening of concrete under multiaxial loading conditions, Eindhoven University of Technology, Eindhoven, The Netherlands, 1984.

[50] I. Fischer, B. Pichler, E. Lach, C. Terner, E. Barraud, F. Britz, Compressive strength of cement paste as a function of loading rate: Experiments and engineering mechanics analysis, Cem. Concr. Res. 58 (2014) 186–200.

[51] H. Zhang, Y. Xu, Y. Gan, E. Schlangen, B. Šavija, Experimentally validated meso-scale fracture modelling of mortar using output from micromechanical models, Cem. Concr. Compos. 110 (2020) 103567.

[52] R.J.-M. Pellenq, A. Kushima, R. Shahsavari, K.J. Van Vliet, M.J. Buehler, S. Yip, F.-J. Ulm, A realistic molecular model of cement hydrates, Proc. Natl. Acad. Sci. U. S.A. 106 (38) (2009) 16102–16107.

[53] D. Hou, J. Yu, P.J.C.P.B.E. Wang, Molecular dynamics modeling of the structure, dynamics, energetics and mechanical properties of cement-polymer nanocomposite, 162 (2019) 433–444.

[54] H. Manzano, J. Dolado, A. Ayuela, Elastic properties of the main species present in Portland cement pastes, Acta Mater. 57 (5) (2009) 1666–1674.

[55] D. Hou, J. Zhang, W. Pan, Y. Zhang, Z. Zhang, Nanoscale mechanism of ions immobilized by the geopolymer: a molecular dynamics study, JNuM 528 (2020) 151841.

[56] D. Hou, Y. Zhu, Y. Lu, Z.J.M.C. Li, Physics, Mechanical properties of calcium silicate hydrate (C–S–H) at nano-scale: a molecular dynamics study, 146(3) (2014) 503-511.

[57] D. Hou, H. Ma, Y. Zhu, Z.J.A.m. Li, Calcium silicate hydrate from dry to saturated state: structure, dynamics and mechanical properties, 67 (2014) 81-94.

[58] M. Hlobil, V. Šmilauer, G. Chanvillard, Micromechanical multiscale fracture model for compressive strength of blended cement pastes, Cem. Concr. Res. 83 (2016) 188–202.

[59] B. Pichler, C. Hellmich, Upscaling quasi-brittle strength of cement paste and mortar: a multi-scale engineering mechanics model, Cem. Concr. Res. 41 (5) (2011) 467–476.